J Nondestruct Eval (2017) 36:19
DOI 10.1007/s10921-017-0397-5

Modelling of Ultrasonic Bulk Wave Scattering by an Axial Crack in a Pipe

Jacob Rubenson[1] · **Anders Boström**[1]

Received: 3 June 2016 / Accepted: 1 February 2017 / Published online: 21 February 2017

Abstract Modelling of ultrasonic bulk wave scattering by an internal, infinitely long, axial crack in a thick-walled pipe is considered. The problem is formulated as a hypersingular integral equation for the crack-opening displacement (COD), the hypersingularity arises in the Green's tensor. The COD is expanded in Chebyshev functions which have the correct square-root singularity along the crack edges, thereby regularizing the integral equation. To discretize the integral equation it is likewise projected onto the same Chebyshev functions. A model of an ultrasonic rectangular vertically polarized shear wave contact probe is developed, and the signal response is calculated using a reciprocity argument. Some numerical examples demonstrate the possible application of the method, in particular investigating the importance of the pipe curvature.

Keywords Non-destructive testing · Wave propagation · Cylindrical geometry · Pipe · Crack

1 Introduction

Ultrasonic nondestructive testing (NDT) is routinely used in some branches of industry, examples being aerospace and nuclear power industries. For a few decades mathematical models of the testing have led to more or less refined theories for varying test situations. There are many benefits from a reliable and validated model. It is easy to perform parametric studies with a model, and it is thus a useful tool in the development of testing procedures. A model can also enhance the physical "feeling", i.e. to know a priori when certain parameters are important, and be a useful educational tool. A good model is also a prerequisite when attempting to solve inverse problems.

One important area of application of ultrasonic NDT is the testing of pipes. This can involve the long-range investigation of corrosion and cracks in pipelines. Then guided waves of relatively low frequencies are used, and in this field a lot of work has been performed, see e.g. Bai et al. [3], Benmeddour et al. [4], Fletcher et al. [9] and Duan and Kirby [8]. It should be noted that the field of guided waves has been active for quite some time, i.e. Rose et. al [11]. Velichko and Wilcox [13] have investigated the relationship between guided wave solutions for plates and pipes. However, there is also an interest in testing of pipes at higher frequencies where guided waves are no longer a useful concept. This is, in particular, of importance in the nuclear power industry where a lot of thick-walled pipes are being tested. For modelling purposes this testing is often approximated as taking place in a plate, but this is not always a valid approximation. Thus there is an interest in modelling ultrasonic testing for defects in pipes when the frequency is in an intermediate range so that neither a guided wave approach nor a plate approximation is applicable. Very little work seems to have been done in this area, although Olsson [10] considers the scattering by a defect in a pipe at low and intermediate frequencies using what may be called a T matrix approach. This work considers the wave scattering inside a thick-walled cylinder by a spherical cavity, excited by a point force.

In the present paper a model of ultrasonic testing for an interior axial crack in a pipe is developed using an integral equation approach. The crack is for simplicity taken as infinitely long in the axial direction, but in practice it

✉ Jacob Rubenson
Jacob.Rubenson@chalmers.se

Anders Boström
anders.bostrom@chalmers.se

[1] Chalmers University of Technology, Gothenburg, Sweden

is enough if the crack is longer than the width of the lobe from the transmitting ultrasonic probe. A realistic model of an ordinary contact probe is used, both in transmission and reception, the latter through a reciprocity argument. The method starts from a hypersingular integral equation over the crack which contains the Green's tensor of the pipe. The free (singular) part of this Green's tensor is expanded in plane waves in the crack coordinate system whereas the part added to fulfill the boundary conditions on the pipe walls are expanded in cylindrical waves. This type of approach has large similarities with the work by Bövik and Boström [7] where the same approach is taken for a crack in a plate.

The method used in this article can be summarized as starting from an integral representation, Eq. (4), contains the Green's tensor for the pipe, Eq. (16) and the crack opening displacement (COD). The traction operator is applied to the integral representation and the field point is taken to the crack surface, however, if the limit is taken inside the integral the integral become improper, Eq. (17). To regularize the integral, and allowing the limit to be taken inside the integral, the integral equation is projected on a set of Chebyshev functions and as a Fourier transform. The COD is expanded in a similar manner. The projection of the integral equation and expansion of the COD integration over the crack surface leads to an equation for the unknown coefficients for the COD, Eq. (29). The incoming field is modelled using a probe model, Eq. (32), derived by Boström and Wirdelius. When the COD and incoming field are fully known a reciprocal argument is used to calculate the signal response in Eq. (40).

2 Formulation of the Scattering Problem

This section contains the statement of the scattering problem and the introduction of the cylindrical basis functions and the integral representation. First consider the geometry, which is a cylindrical pipe with inner and outer surfaces at radii r_i and r_o on surfaces S_i and S_o. Both Cartesian coordinates x, y, z and cylindrical coordinates r, φ, z are used. The open internal crack is infinitely long in the axial direction and is placed at $\varphi = 0$ between $r = a$ and $r = b$, and the crack surface is denoted S_c, see Fig. 1. The material of the pipe is assumed to be isotropic and homogeneous with Lamé parameters λ and μ and density ρ. The equation of motion for the displacement field, $\mathbf{u}$, in an elastic solid is (Achenbach [1]),

$$k_p^{-2}\nabla\nabla\cdot\mathbf{u}(\mathbf{r}) - k_s^{-2}\,\nabla\wedge\nabla\wedge\mathbf{u}(\mathbf{r}) + \mathbf{u}(\mathbf{r}) = \mathbf{0}. \tag{1}$$

It should be noted that only a single frequency, ω, is considered and that the factor $\exp(-\mathrm{i}\omega t)$ is suppressed. The longitudinal wave number is $k_p^2 = \rho\omega^2/(2\mu+\lambda)$ and the transverse is $k_s^2 = \rho\omega^2/\mu$. The displacement field can be divided into an incoming part and a scattered part

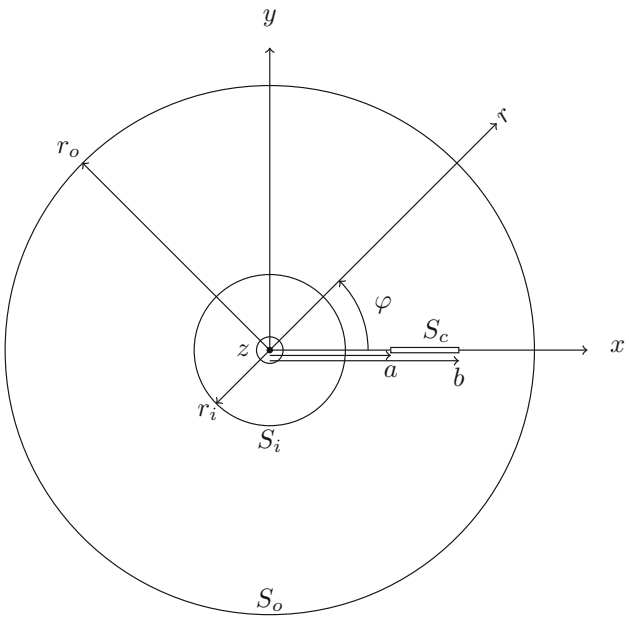

Fig. 1 The geometry of the pipe with inner radius r_i and outer radius r_o and the crack situated on the x axis between $x = a$ and $x = b$

$$\mathbf{u} = \mathbf{u}^{\mathrm{in}} + \mathbf{u}^{\mathrm{sc}}, \tag{2}$$

where the incoming part $\mathbf{u}^{\mathrm{in}}$ is the field that exists in the pipe in the absence of the crack and the scattered part $\mathbf{u}^{\mathrm{sc}}$ is the extra field needed to satisfy the boundary condition on the crack. The fields in the pipe are excited by an ultrasonic probe on the outer surface of the pipe, and this is modelled as a traction boundary condition, discussed in detail later. Otherwise all the surfaces of the pipe and the crack surface are traction free. To completely specify the problem radiation conditions are also needed, these state that energy must be outgoing far away from the probe.

Solutions in the form of outgoing cylindrical vector wave functions to the equation of motion (1) in cylindrical coordinates can be expressed as [6]

$$\begin{aligned}
\boldsymbol{\chi}_{1\sigma m}(h;\mathbf{r}) &= \sqrt{\frac{\epsilon_m}{8\pi}}\frac{1}{q_s}\nabla\wedge\left(\hat{z}\mathrm{H}_m(rq_s)e^{\mathrm{i}hz}\begin{Bmatrix}\sin(m\varphi)\\ \cos(m\varphi)\end{Bmatrix}\right),\\
\boldsymbol{\chi}_{2\sigma m}(h;\mathbf{r}) &= \sqrt{\frac{\epsilon_m}{8\pi}}\\
&\quad\times\frac{1}{q_s k_s}\nabla\wedge\nabla\wedge\left(\hat{z}\mathrm{H}_m(rq_s)e^{\mathrm{i}hz}\begin{Bmatrix}\sin(m\varphi)\\ \cos(m\varphi)\end{Bmatrix}\right),\\
\boldsymbol{\chi}_{3\sigma m}(h;\mathbf{r}) &= \sqrt{\frac{\epsilon_m}{8\pi}}\frac{k_p}{k_s^3}\nabla\left(\mathrm{H}_m(rq_p)e^{\mathrm{i}hz}\begin{Bmatrix}\sin(m\varphi)\\ \cos(m\varphi)\end{Bmatrix}\right).
\end{aligned} \tag{3}$$

Here, H_m is a Hankel function of the first kind and of order m, this set of basis functions represents outwards traveling waves. There are also regular waves ($\mathrm{Re}\,\boldsymbol{\chi}_{\tau\sigma m}$), which are obtained by replacing the Hankel functions with Bessel func-

tions, J_m. The Neumann factor is defined as $\epsilon_m = 2 - \delta_{m0}$, h is the axial wave number and the radial wave numbers are defined as $q_i = (k_i^2 - h^2)^{1/2}$, $i = p, s$. The radial wave numbers are chosen to have a non-negative imaginary part. The basis functions have several indices that represent the mode ($\tau = 1, 2, 3$), parity ($\sigma = o, e$) and order ($m = 0, 1, 2\ldots$), which are combined to a multi-index, $\boldsymbol{\chi}_k \equiv \boldsymbol{\chi}_{\tau\sigma m}$. The first two modes are shear waves ($\tau = 1, 2$) and the third is a pressure wave ($\tau = 3$), the parity is determined by the parity of the trigonometric function. These basis functions can be divided into two groups $\tau\sigma = 1o2e3e$ (symmetric in φ) and $\tau\sigma = 1e2o3o$ (anti-symmetric in φ). The basis functions will be used to construct the Green's tensor for the cylindrical pipe and to expand the incoming field produced by the probe.

A way to solve the scattering problem is to start with an integral representation (see Ström [12] for a discussion of integral formulations)

$$\mathbf{u}^{\text{in}}(\mathbf{r}') + \frac{k_s}{\mu}\int_{S_c} \mathrm{d}S\,\Delta\mathbf{u}(\mathbf{r})\cdot\mathbf{t}^{(\varphi)}(\mathsf{G}(\mathbf{r},\mathbf{r}')) = \begin{cases} 0, & \mathbf{r}' \notin (V) \\ \mathbf{u}(\mathbf{r}'), & \mathbf{r}' \in (V) \end{cases}, \tag{4}$$

where $\mathbf{r}'$ is the field point and $\mathbf{r}$ the integration variable over the crack. The unknown crack opening displacement (COD) $\Delta\mathbf{u}(\mathbf{r})$ is the jump in displacement across the crack and the traction operator is defined as

$$\mathbf{t}^{(n)}(\mathbf{u}) = \hat{n}\lambda\nabla\cdot\mathbf{u} + 2\mu\hat{n}\cdot\nabla\mathbf{u} + \mu\hat{n}\wedge(\nabla\wedge\mathbf{u}). \tag{5}$$

The Green's tensor is here chosen as the one of the pipe, i.e. it satisfies the boundary conditions on the inner and outer surfaces of the pipe, and therefore the integral is only over the surface of the crack S_c.

3 Green's Tensors

In this section the Green's tensor, $\mathsf{G}(\mathbf{r},\mathbf{r}')$ for the pipe is derived. The Green's tensor satisfies

$$k_p^{-2}\nabla\nabla\cdot\mathsf{G}(\mathbf{r},\mathbf{r}') - k_s^{-2}\nabla\wedge\nabla\wedge\mathsf{G}(\mathbf{r},\mathbf{r}') + \mathsf{G}(\mathbf{r},\mathbf{r}') = -k_s^3\mathsf{I}\delta(\mathbf{r}-\mathbf{r}'), \tag{6}$$

and the traction free boundary conditions on the inner and outer surfaces of the pipe. Here I is the unit dyadic. Also the radiation condition must be satisfied, meaning that the energy must be outward propagating far away from the point force that is the source for the Green's tensor. To derive the Green's tensor for the pipe it is convenient to divide it into two parts. The first part is the free space Green's tensor that takes care of the singularity and the other part is the regular part that is needed to fulfil the boundary conditions on the pipe. The boundary conditions for the free space Green's tensor are radiation conditions, and the free space Green's tensor can be expressed as [7]

$$\mathsf{G}^{\text{sing}}(\mathbf{r},\mathbf{r}') = 2\mathrm{i}\sum_{j=1}^{3}\int_{-\infty}^{\infty}\int_{-\infty}^{\infty}\frac{\mathrm{d}q\,\mathrm{d}p}{k_j h_j}\mathbf{f}_j\mathbf{f}_j^* e^{\mathrm{i}(h_j|y-y'|+q(z-z')+p(x-x'))}, \tag{7}$$

using Cartesian coordinates, where the x-coordinate is aligned with the crack as seen in Fig. 1. The quantities f_{jn}, f_{jn}^* are defined as

$$\mathbf{f}_1 = \frac{\mathrm{i}}{4\pi s}(p, 0, q), \tag{8}$$

$$\mathbf{f}_2 = \frac{1}{4\pi s k_s}\left(qh_s, -s^2, -ph_s\right), \tag{9}$$

$$\mathbf{f}_3 = \frac{\mathrm{i}}{4\pi}\sqrt{\frac{k_p}{k_s^3}}\left(-q, -h_p, p\right). \tag{10}$$

(It should be noted that these are not the same as in Bövik and Boström [7], the order has been permuted since the coordinate axes are different.) The quantity k_i is the wave number k_p or k_s which is used to define $h_j = \sqrt{k_j^2 - s^2}$, where the branch cut $\mathrm{Im}(h_j) > 0$ is chosen. This is a double Fourier transform representation in x and z of the Green's tensor.

The free space Green's tensor can also be expressed as in cylindrical coordinates [6]

$$\mathsf{G}^{\text{sing}}(\mathbf{r},\mathbf{r}') = \mathrm{i}\sum_k\int_{-\infty}^{\infty}\frac{\mathrm{d}h}{k_s}\boldsymbol{\chi}_k(h;\mathbf{r}_>)\mathrm{Re}\boldsymbol{\chi}_k^{\dagger}(h;\mathbf{r}_<), \tag{11}$$

where the outgoing and regular cylindrical wave functions defined in Eq. (3) are used. The dagger symbol (†) represents a change of sign of i to $-$i in the basis functions and $\mathbf{r}_>$ ($\mathbf{r}_<$) is the choice of $\mathbf{r}$ or $\mathbf{r}'$ with the largest (smallest) radial component. These two representations for the free space Green's tensors are used to create the Green's tensor for the pipe. The two representations of the free space Green's tensors are used since the crack is best expressed in rectangular coordinates while it is necessary to calculate the reflections from the cylinder walls in cylindrical coordinates.

To find an expression for the regular part of the Green's tensor a method for deriving the reflections for an elastic displacement field within a cylindrical pipe is considered. Olsson [10] derived an expression for the reflected displacement field, $\mathbf{u}^{\text{refl}}$, for any excitation

$$\begin{aligned}\mathbf{u}^{\text{refl}}(\mathbf{r}) \;=& \sum_{kk'} \int_{-\infty}^{\infty} \frac{\mathrm{d}h}{k_s} \Big(-\boldsymbol{\chi}_k(h;\mathbf{r}\,) M^3_{kk'}(h) a^0_{k'}(h) \\ &+ \boldsymbol{\chi}_k(h;\mathbf{r}\,) M^4_{kk'}(h) a^2_{k'}(h) \\ &+ \mathrm{Re}\boldsymbol{\chi}_k(h;\mathbf{r}\,) M^1_{kk'}(h) a^0_{k'}(h) \\ &- \mathrm{Re}\boldsymbol{\chi}_k(h;\mathbf{r}\,) M^2_{kk'}(h) a^2_{k'}(h) \Big). \end{aligned} \tag{12}$$

Here $M^{\nu}_{kk'}$ ($\nu = 1, 2, 3, 4$) are matrices defined by Olsson [10] and the geometrical interpretation of them are reflections for the different waves starting from either the inner or outer surface. The quantities a^0_k and a^2_k are quantities from an expansion of the excitation in the cylindrical waves. The expansion in a^0_k is valid inside the inner surface of the cylinder, where $r < r_i$, whereas the expansion in a^2_k is valid outside the outer surface, $r > r_o$. As the source for the Green's tensor is a point force, its expansion in cylindrical waves is exactly the free space Green's tensor (11), so the following expansion coefficients are obtained

$$\mathbf{a}^0_k = i\,\boldsymbol{\chi}^{\dagger}_k(\mathbf{r}\,'), \tag{13}$$

$$\mathbf{a}^2_k = \mathrm{i}\mathrm{Re}\boldsymbol{\chi}^{\dagger}_k(\mathbf{r}\,'). \tag{14}$$

It should be noted that there are some differences compared to Olsson [10] due to different normalizations. The regular part of the Green's tensor thus becomes

$$\begin{aligned}&\mathsf{G}^{\text{reg}}(\mathbf{r};\mathbf{r}\,') \\ &= \mathrm{i} \sum_{kk'} \int_{-\infty}^{\infty} \frac{\mathrm{d}h}{k_\tau} \Big(-\boldsymbol{\chi}_k(h;\mathbf{r}\,) M^3_{kk'}(h) \boldsymbol{\chi}^{\dagger}_{k'}(h;\mathbf{r}\,') \\ &\quad + \boldsymbol{\chi}_k(h;\mathbf{r}\,) M^4_{kk'}(h) \mathrm{Re}\boldsymbol{\chi}^{\dagger}_{k'}(h;\mathbf{r}\,') \\ &\quad + \mathrm{Re}\boldsymbol{\chi}_k(h;\mathbf{r}\,) M^1_{kk'}(h) \boldsymbol{\chi}^{\dagger}_{k'}(h;\mathbf{r}\,') \\ &\quad - \mathrm{Re}\boldsymbol{\chi}_k(h;\mathbf{r}\,) M^2_{kk'}(h) \mathrm{Re}\boldsymbol{\chi}^{\dagger}_{k'}(h;\mathbf{r}\,') \Big). \end{aligned} \tag{15}$$

The total Green's tensor for the pipe can now be constructed as the sum of (7) and (15) as

$$\mathsf{G}(\mathbf{r};\mathbf{r}\,') = \mathsf{G}^{\text{sing}}(\mathbf{r};\mathbf{r}\,') + \mathsf{G}^{\text{reg}}(\mathbf{r};\mathbf{r}\,'). \tag{16}$$

4 The Integral Equation

To solve the scattering problem an integral equation on the crack is now derived from the integral representation Eq. (4). Applying the traction operator to the integral representation and letting the field point approach the crack surface gives

$$\begin{aligned}&\mathbf{t}^{(\varphi)}(\mathbf{u}^{\text{in}}(r', 0, z')) \\ &= -\lim_{\varphi' \to 0} \frac{k_s}{\mu} \int_{S_c} \mathrm{d}S\, \Delta\mathbf{u}(\mathbf{r}) \cdot \Sigma(r, 0, z; r', \varphi', z'), \end{aligned} \tag{17}$$

Here Σ is the double stress tensor which is obtained by applying the traction operator twice to the Green's tensor with respect to both the primed and the unprimed coordinates. Note that the integral equation is of hypersingular type; it is thus not possible to take the limit inside the integral. The singular part of the double stress tensor is

$$\begin{aligned}&\Sigma^{\text{sing}}(\mathbf{r};\mathbf{r}\,') \\ &= 2\mathrm{i} \sum_{j=1}^{3} \int_{-\infty}^{\infty} \int_{-\infty}^{\infty} \frac{\mathrm{d}q\,\mathrm{d}p}{k_j h_j} \mathbf{F}_j \mathbf{F}^*_j e^{\mathrm{i}(h_j|y-y'|+q(z-z')+p(x-x'))}, \end{aligned} \tag{18}$$

where (again permuted components as compared to Bövik and Boström [7] since the coordinates are permuted)

$$\mathbf{F}_1 = \frac{1}{4\pi s} \left(p h_s, 0, q h_s \right), \tag{19}$$

$$\mathbf{F}_2 = \frac{\mathrm{i}}{4\pi s k_s} \left(qK, -2s^2 h_s, -pK \right), \tag{20}$$

$$\mathbf{F}_3 = \frac{1}{4\pi} \sqrt{\frac{k_p}{k_s^3}} \left(-2q h_p, -K, 2p h_p \right), \tag{21}$$

$$K = 2s^2 - k_s^2. \tag{22}$$

The regular part of the double stress tensor directly becomes

$$\begin{aligned}&\Sigma^{\text{reg}}(\mathbf{r};\mathbf{r}\,') \\ &= \mathrm{i} \sum_{kk'} \int_{-\infty}^{\infty} \frac{\mathrm{d}h}{k_s} \Big(-\mathbf{t}^{(\varphi')}(\boldsymbol{\chi}_k(h;\mathbf{r}\,')) M^3_{kk'}(h) \mathbf{t}^{(\varphi)}(\boldsymbol{\chi}^{\dagger}_{k'}(h;\mathbf{r})) \end{aligned} \tag{23}$$

$$\begin{aligned}&\quad + \mathbf{t}^{(\varphi')}(\boldsymbol{\chi}_k(h;\mathbf{r}\,')) M^4_{kk'}(h) \mathbf{t}^{(\varphi)}(\mathrm{Re}\boldsymbol{\chi}^{\dagger}_{k'}(h;\mathbf{r})) \\ &\quad + \mathbf{t}^{(\varphi')}(\mathrm{Re}\boldsymbol{\chi}_k(h;\mathbf{r}\,')) M^1_{kk'}(h) \mathbf{t}^{(\varphi)}(\boldsymbol{\chi}^{\dagger}_{k'}(h;\mathbf{r})) \\ &\quad - \mathbf{t}^{(\varphi')}(\mathrm{Re}\boldsymbol{\chi}_k(h;\mathbf{r}\,')) M^2_{kk'}(h) \mathbf{t}^{(\varphi)}(\mathrm{Re}\boldsymbol{\chi}^{\dagger}_{k'}(h;\mathbf{r})) \Big) \end{aligned} \tag{24}$$

The tractions of the cylindrical wave functions are straightforward to calculate. The double stress tensor in Eq. (17) is then obtained by adding the singular and regular parts.

The singular part of the pipe's Green's tensor Eq. (7) gives a hypersingular part in the integral equation, Eq. (17), which must be handled before the limit can be moved inside the integral. To this end the crack opening displacement is expanded in the following set of functions (defined on the interval $[-1, 1]$)

$$\psi_m(s) = \begin{cases} -\frac{1}{\pi m} \cos(m \arcsin(s)), & m = 1, 3, \ldots \\ \frac{\mathrm{i}}{\pi m} \sin(m \arcsin(s)), & m = 2, 4, \ldots \end{cases}, \tag{25}$$

These Chebyshev functions constitute an orthogonal set of functions and they have the same square root behavior [7]

at the edges of the crack as the COD should have. Another reason for using them is the following convenient property

$$\int_{-1}^{1} \mathrm{d}s\ \psi_m(s) e^{\mathrm{i}\gamma s} = \frac{-1}{\gamma} \mathrm{J}_m(\gamma), \tag{26}$$

where γ is any complex number. The COD, $\Delta\mathbf{u}$, is thus expanded in a series in Chebyshev functions, and also as a Fourier transform in z, in the following way

$$\Delta\mathbf{u} = \sum_{n=1}^{\infty} \int_{-\infty}^{\infty} \frac{\mathrm{d}p}{k_s} \boldsymbol{\beta}_n(p) \psi_n(g(r)) e^{\mathrm{i}pz}, \tag{27}$$

where β_{nj} are the unknown expansion functions to be determined. The function $g(r)$ takes care of the linear transformation from the interval $[-1, 1]$ to the crack interval $[a, b]$.

The integral equation is projected onto the Chebyshev functions and a Fourier transform in z is also taken to yield

$$\begin{aligned}
&\int_{S_c} \mathrm{d}S\ \psi_n(g(r')) e^{-\mathrm{i}pz'} \mathbf{t}^{(\varphi)}(\mathbf{u}^{\mathrm{in}}(r', 0, z')) \\
&\quad = -\frac{k_s}{\mu} \int_{S_c} \mathrm{d}S\ \psi_n(g(r')) e^{-\mathrm{i}pz'} \\
&\qquad \times \lim_{\varphi' \to 0} \int_{S_c} \mathrm{d}S \sum_{n'=1}^{\infty} \int_{-\infty}^{\infty} \frac{\mathrm{d}p'}{k_s} \boldsymbol{\beta}_{n'}(p') \psi_{n'}(g(r)) e^{\mathrm{i}p'z} \\
&\qquad \cdot \Sigma(r, 0, z; r', \varphi', z').
\end{aligned} \tag{28}$$

In this process the singularity of the Green's tensor is regularized and the limit can be taken inside the integral. It is now possible to evaluate some of the integrals and after some manipulations a system of equations for the COD coefficients, $\beta_{nj}(p)$ can be establish as follows

$$\sum_{n'j'} Q_{njn'j'}(p) \beta_{n'j'}(p) = U_{nj}(p), \tag{29}$$

where the system matrix is

$$\begin{aligned}
Q_{njn'j'} &= 8\pi^2 \mathrm{i} k_s \sum_{l=1}^{3} \int_{-\infty}^{\infty} \frac{\mathrm{d}q}{k_l h_l q^2} F_{jl} F_{j'l} \\
&\quad \times \mathrm{J}_n\left(\frac{q(b-a)}{2}\right) \mathrm{J}_{n'}\left(\frac{q(b-a)}{2}\right) \\
&\quad + \frac{4\pi^2 \mathrm{i}}{\mu^2} \sum_{kk'} \int_a^b \int_a^b \mathrm{d}r' \mathrm{d}r \psi_{n'}(g(r)) \psi_n(g(r')) \\
&\quad \times \Big(- T_{jk}^{+}(-p, r') M_{kk'}^{3}(-p) \overline{T}_{j'k'}^{+}(-p, r) \\
&\quad + T_{jk}^{+}(-p, r') M_{kk'}^{4}(-p) \overline{T}_{j'k'}^{0}(-p, r) \\
&\quad + T_{jk}^{0}(-p, r') M_{kk'}^{1}(-p) \overline{T}_{j'k'}^{+}(-p, r) \\
&\quad - T_{jk}^{0}(-p, r') M_{kk'}^{2}(-p) \overline{T}_{j'k'}^{0}(-p, r) \Big),
\end{aligned} \tag{30}$$

and the right-hand side is

$$U_{jn}(p) = \frac{k_s}{\mu} \int_{-\infty}^{\infty} \int_a^b \mathrm{d}z' \mathrm{d}r'\ t_j^{(\varphi)}(\mathbf{u}^{\mathrm{in}}) \psi_n(g(r')) e^{-\mathrm{i}pz'}. \tag{31}$$

Here the following notation is introduced: $T_{jk}^{+}(p; r) = t_n^{(}\varphi)(\boldsymbol{\chi}_k(p; \mathbf{r}))|_{z=\varphi=0}$; the outgoing waves are identified with a plus sign, incoming waves are identified with a zero, and the dagger operator is indicated with an overline. It can be noted that for the singular part the integral property in (26) has been used twice. The right-hand side $U_{jn}(p)$ is due to the traction on the crack from the incoming field $\mathbf{u}^{\mathrm{in}}$, i.e. the field in the absence of the crack, and this is discussed in the next section. Solving the system of linear equations for the COD expansion coefficients $\beta_{n',j'}(p)$ fully determines the COD and thus the scattered field.

5 Transmitting and receiving probes

The model of the transmitting probe is similar to the one used by Boström and Wirdelius [5] to model a probe on a planar surface. The action of the probe is thus modelled as an applied traction as the boundary condition where the probe is located. The field from the transmitting probe is obtained by determining the displacement field induced by this given set of boundary conditions, in the absence of a defect.

Here this model is modified to a cylindrical surface. The boundary conditions for the incoming field ($\mathbf{u}^{\mathrm{in}}$, i.e. the field in the absence of the crack, is thus

$$\mathbf{t}^{(r)}(\mathbf{u}^{\mathrm{in}}(\mathbf{r})) = \begin{cases} \hat{r}\mathrm{i}\mu k_s \exp(-\mathrm{i}k_s r_o \sin(\gamma)(\varphi - \varphi_0)), & \mathbf{r} \in S_1 \\ 0, & \mathbf{r} \notin S_1 \end{cases}, \tag{32}$$

$$S_1 = \{\varphi \in [\varphi_0 - \delta, \varphi_0 + \delta], z \in [-\zeta, \zeta]\},$$

Note that only the normal component (pressure) is taken as nonzero (although there is no difficulty to include also tangential components, see Boström and Wirdelius [5]), the other components and the traction on the inner surface of the pipe are zero. Here ζ is the half length of the probe in the axial direction, δ is the half width of the probe in the angular direction, and φ_0 is the probe position, see Fig. 2. The variable γ is the angle of the probe as measured from the normal direction, see Fig. 2. The probe model can be changed from a shear probe to a pressure probe by change the shear wave number (k_s) to the pressure wave number (k_p) in the exponential.

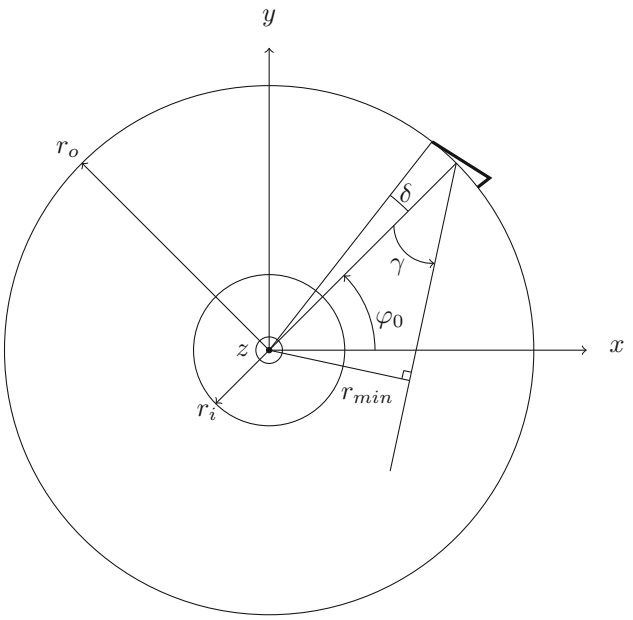

Fig. 2 The probe is placed at the outer surface at the angle φ_0, the angle of the probe is γ, the width of the probe is 2δ and the length of the probe is 2ζ in the axial direction

To obtain the incoming displacement field, $\mathbf{u}^{\text{in}}$, from these boundary condition the following ansatz for the displacement field is made

$$\mathbf{u}^{\text{in}} = \sum_k \int_{-\infty}^{\infty} \frac{\mathrm{d}h}{k_\tau} \left(\xi_k^1 \boldsymbol{\chi}_k + \xi_k^2 \,\mathrm{Re}\boldsymbol{\chi}_k \right), \tag{33}$$

where the coefficients ξ_k^1 and ξ_k^2 are to be determined. To solve for these unknowns the traction operator in the normal direction is applied and the boundary conditions are used to obtain

$$\begin{aligned} &\sum_k \int_{-\infty}^{\infty} \frac{\mathrm{d}h}{k_\tau} \left(\xi_k^1 \mathbf{t}^{(r)}(\boldsymbol{\chi}_k) + \xi_k^2 \mathbf{t}^{(r)}(\mathrm{Re}\boldsymbol{\chi}_k) \right) \\ &\quad = \mathbf{t}^{(r)}(\mathbf{u}^{\text{in}}), \quad r = r_o, \end{aligned} \tag{34}$$

$$\begin{aligned} &\sum_k \int_{-\infty}^{\infty} \frac{\mathrm{d}h}{k_\tau} \left(\xi_k^1 \mathbf{t}^{(r)}(\boldsymbol{\chi}_k) + \xi_k^2 \mathbf{t}^{(r)}(\mathrm{Re}\boldsymbol{\chi}_k) \right) \\ &\quad = \mathbf{0}, \quad r = r_i. \end{aligned} \tag{35}$$

Expanding the right-hand side of these equations in a Fourier series in the angular direction and a Fourier transform in the axial direction the following system of equations is obtained for the coefficients on the outer pipe surface $r = r_o$

$$\begin{aligned}
&\xi_{1om}^1 T_{1orm}^+ + \xi_{2em}^1 T_{2erm}^+ + \xi_{3em}^1 T_{3erm}^+ + \xi_{1om}^2 T_{1orm}^0 \\
&\quad + \xi_{2em}^2 T_{2erm}^0 + \xi_{3em}^2 T_{3erm}^0 = A_{em}, \\
&\xi_{1em}^1 T_{1erm}^+ + \xi_{2om}^1 T_{2orm}^+ + \xi_{3om}^1 T_{3orm}^+ + \xi_{1em}^2 T_{1erm}^0 \\
&\quad + \xi_{2om}^2 T_{2orm}^0 + \xi_{3om}^2 T_{3orm}^0 = A_{om}, \\
&\xi_{1em}^1 T_{1e\varphi m}^+ + \xi_{2om}^1 T_{2o\varphi m}^+ + \xi_{3om}^1 T_{3o\varphi m}^+ + \xi_{1em}^2 T_{1e\varphi m}^0 \\
&\quad + \xi_{2om}^2 T_{2o\varphi m}^0 + \xi_{3om}^2 T_{3o\varphi m}^0 = 0, \\
&\xi_{1om}^1 T_{1o\varphi m}^+ + \xi_{2em}^1 T_{2e\varphi m}^+ + \xi_{3em}^1 T_{3e\varphi m}^+ + \xi_{1om}^2 T_{1o\varphi m}^0 \\
&\quad + \xi_{2em}^2 T_{2e\varphi m}^0 + \xi_{3em}^2 T_{3e\varphi m}^0 = 0, \\
&\xi_{1em}^1 T_{1ezm}^+ + \xi_{2om}^1 T_{2ozm}^+ + \xi_{3om}^1 T_{3ozm}^+ + \xi_{1em}^2 T_{1ezm}^0 \\
&\quad + \xi_{2om}^2 T_{2ozm}^0 + \xi_{3om}^2 T_{3ozm}^0 = 0, \\
&\xi_{1om}^1 T_{1ozm}^+ + \xi_{2em}^1 T_{2ezm}^+ + \xi_{3em}^1 T_{3ezm}^+ + \xi_{1om}^2 T_{1ozm}^0 \\
&\quad + \xi_{2em}^2 T_{2ezm}^0 + \xi_{3em}^2 T_{3ezm}^0 = 0.
\end{aligned}$$

Here the dependence from the wave functions is contained in $T_{\tau\sigma jm}^+$, the radial dependence is omitted for brevity (but it is important to note that the equations are valid on the outer surface of the cylinder). There is no significant difference on the inner surface of the cylinder except that the radial coordinate is different and that the right-hand side is zero. The right-hand side can be written as

$$\begin{aligned}
A_{om} = &\big[\mathrm{i}m \cos(m(\varphi_0 + \delta)) \\
&+ \exp(2\mathrm{i}A\delta) \big\{ -\mathrm{i}m \cos(m(\varphi_0 - \delta)) \\
&+ A \sin(m(\varphi_0 - \delta)) \big\} \\
&- A \sin(m(\varphi_0 + \delta)) \big] \frac{2B \sin(h\zeta)}{h} \frac{\exp(-\mathrm{i}A\delta)}{A^2 - m^2}.
\end{aligned} \tag{36}$$

$$\begin{aligned}
A_{em} = &\big[-A \cos(m(\varphi_0 + \delta)) \\
&+ \exp(2\mathrm{i}A\delta) \big\{ A \cos(m(+\varphi_0 - \delta)) \\
&+ \mathrm{i}m \sin(m(-\varphi_0 + \delta)) \big\} \\
&- \mathrm{i}m \sin(m(\varphi_0 + \delta)) \big] \frac{2B \sin(h\zeta)}{h} \frac{\exp(-\mathrm{i}A\delta)}{A^2 - m^2},
\end{aligned} \tag{37}$$

where $A = k_s r_o \sin(\gamma)$ and $B = \mathrm{i}\mu k_s$, m is the Fourier series number, and h is the Fourier transform variable. Twelve equations are thus obtained to solve for the twelve expansion coefficients ξ_k^1 and ξ_k^2.

To model a receiving probe the reciprocal argument developed by Auld [2] is very useful. In the reciprocal argument two elastodynamic states are used, one with the defect present (state 1) and one without the defect (state 2), but both with the pipe present. In state 1 the actual transmitter is acting as transmitter but in state 2 the receiving transmitter is acting as transmitter. The reciprocal argument gives the change in electrical reflection coefficient $\delta\Gamma$ of the receiving probe due to the defect, i.e. more or less the quantity measured, on the following form

$$\delta\Gamma = \frac{\mathrm{i}\omega}{4P} \int_S \mathrm{d}S(\mathbf{u}_1 \cdot \mathbf{t}^{(n)}(\mathbf{u}_2) - \mathbf{u}_2 \cdot \mathbf{t}^{(n)}(\mathbf{u}_1)). \tag{38}$$

Here the surface integral is over a surface surrounding the crack, the normal vector is in the outward direction, and P

is the electric power exciting the elastodynamic field. Collapsing the surface to the crack and using the traction free boundary condition on the crack this is further simplified to

$$\delta\Gamma = \frac{\mathrm{i}\omega}{4P}\int_{S_c} \mathrm{d}S\,\Delta\mathbf{u}\cdot\mathbf{t}^{(\varphi)}(\mathbf{u}^{\mathrm{in}}). \tag{39}$$

Inserting the expansions of the incoming field Eq. (33) and the COD Eq. (27), and formally solving the system of equations Eq. (29) this can be further developed

$$\delta\Gamma(\omega) = \frac{\mathrm{i}\omega\pi^2}{4P\mu}\sum_{n,n',j,j'}\int_{-\infty}^{\infty}\mathrm{d}p\, I_{jn}(p)Q^{-1}_{njn'j'}(p)I_{j'n'}(-p). \tag{40}$$

The integrals

$$I_{jn}(p) = \sum_k \int_a^b \mathrm{d}r\psi_n(g(r))\left(\xi^1_k(p)T^+_{kj}(p) + \xi^2_k(p)T^0_{kj}(p)\right), \tag{41}$$

where $T^+_{kj}(p)$ and $T^0_{kj}(p)$ are defined in Eq. (31), are related to the receiving and transmitting probes. This gives a nice division of the received signal Eq. (40) into three parts, where the first part in the integrand is due to the receiving probe, the second to the crack, and the third to the transmitting probe. As written the reciprocal argument is used with the same probe as both transmitter and receiver, i.e. pulse echo testing, but the same formulation is of course valid if the transmitting and receiving probes are different, but there will be two different $I_{j,n}(p)$ in Eq. (40), one for the transmitter and one for the receiver. It should be noted that only the extra field due to the presence of the crack is included; the field in the pipe in the absence of the crack is thus not present and require additional computations if wanted, but this is not pursued here. The omitted field can of course be important, but the present calculations correspond to a baseline measurement where the deviations from a perfect pipe are monitored.

6 Numerical Examples

A few numerical examples are now provided to illustrate the method presented in this article. Most of the numerics is straightforward, the only part where caution is required is the computation of the q integral in the first term in (30). Due to branch cuts the integral is extended into the complex plane, and the curve which is integrated along is chosen as

$$h = t(1 - \alpha\mathrm{i}\mathrm{e}^{-\beta|t|}), \quad t \in (-\infty, \infty). \tag{42}$$

As the absolute value function is not analytic, the integral has been divided into two integrals at $t = 0$. The two parameters are taken as $\alpha = 1$ and $\beta = \mathrm{Re}(k_s)^{-1}$ as this gives a curve that avoids the branch points sufficiently without going too far into the second and fourth quadrant (where the integrand increases exponentially). Up to 800 integration points are needed in a Gauss-Legendre quadrature. The integrals over the radial coordinates r and r' in (30) are evaluated using a Gauss-Legendre scheme with 50 points. The sums over m that appear in some places are truncated at $m_{\max} = r_o\mathrm{Re}(k_s) + 5$.

Table 1 Minimum radii for the nominal probe ray (r_{min} in Fig. 2) for different probe angles and outer radii, all units are in millimeters

r_o	$r_{\min}$ for γ	30°	45°	60°
40		20.0	28.3	34.6
50		25.0	35.3	43.3
60		30.0	42.4	52.0

The material of the pipe is kept fixed and is chosen as steel with the following material properties: $\mu^\star = 79.3$GPa, $\lambda^\star = 86.6$GPa and $\rho = 7800\mathrm{kgm}^{-3}$. As this is more realistic and as it increases the convergence damping is assumed to be present in the form $\mu = \mu^\star(1 + \mathrm{i}\epsilon)$ and $\lambda = \lambda^\star(1 + \mathrm{i}\epsilon)$, where $\epsilon = 0.01$ is chosen. The probe is scanning in pulse-echo along a quarter circle on the outer surface of the cylinder at 700 positions. The probe is of shear wave type approximately t10mm by 10mm and is operating at the fixed frequency 1MHz. The angle of the probe, γ, is set to 30 °, 45°, or 60°. The signal response is normalized with the largest value for each probe with the same angle, although strictly speaking the probes are not completely identical for different radii of the outer pipe wall. The crack width in the radial direction is chosen as 5mm and it is placed 1mm from the inner wall, so it is practically surface-breaking. To investigate the influence of the curvature of the wall the wall thickness is kept constant and the inner and outer radii are varied. This has been performed for two different wall thicknesses, 10mm and 20mm, and several different inner and outer radii.

A new feature of a pipe, as compared to a plate, is that the ultrasound from an angled probe can only penetrate to a finite depth. Considering the ray in the nominal direction from the probe it can only reach down to the radius $r_{\min} = r_o\sin(\gamma)$, where as before r_o is the radius of the outer pipe surface and γ the angle of the probe. This minimum radius is shown in Table 1 for the outer radii and probe angles considered below in the numerical examples. Particularly for $\gamma = 60°$ the penetration depth is quite moderate, and might for thick-walled pipes be a limiting factor of the usefulness of such a probe.

In Figs. 3, 4, and 5 signal responses are given for pipes with wall thickness 10 mm for probe angles 30°, 45°, and 60°, respectively. Three different outer radii are shown in each figure, namely 40, 50, and 60 mm, and as the wall thickness is constant the corresponding inner radii are 30, 40, and 50 mm,

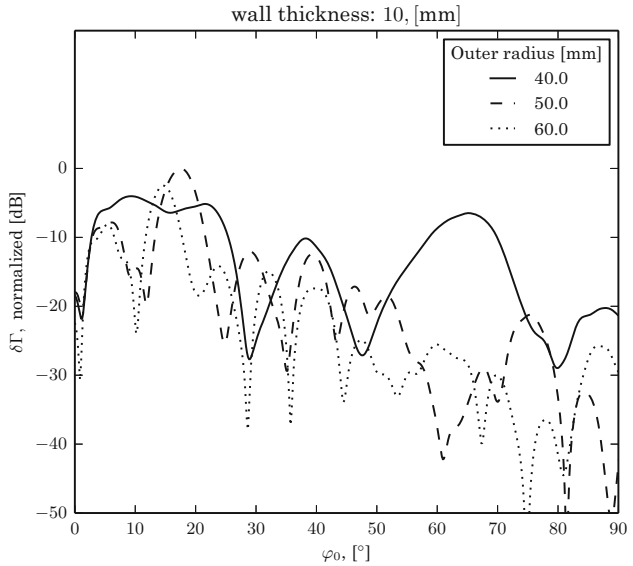

Fig. 3 The signal response $\delta\Gamma$ as a function of the probe position φ_0 for a probe with angle 30°; wall thickness 10*mm* and outer radius between 40mm and 60mm

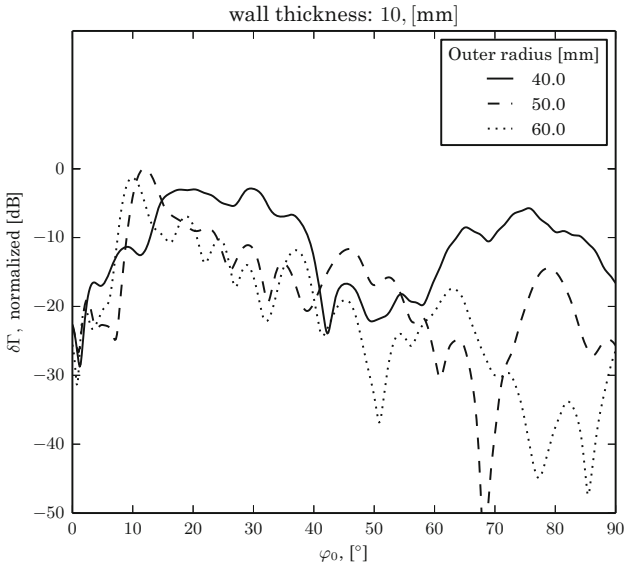

Fig. 5 The signal response $\delta\Gamma$ as a function of the probe position φ_0 for a probe with angle 60°; wall thickness 10mm and outer radius between 40mm and 60mm

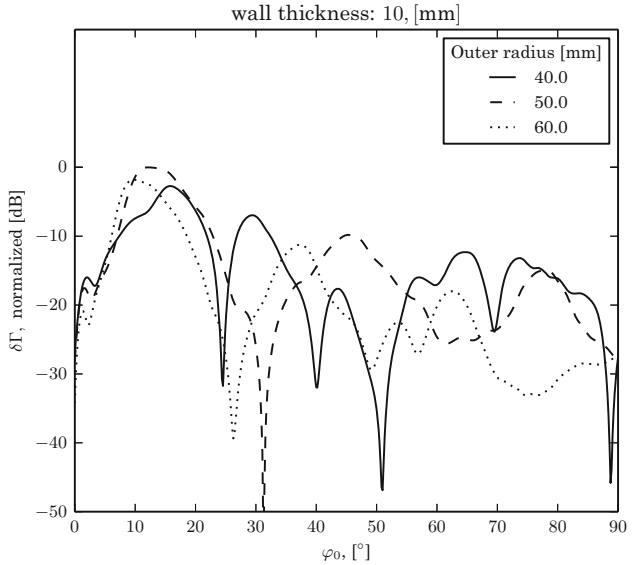

Fig. 4 The signal response $\delta\Gamma$ as a function of the probe position φ_0 for a probe with angle 45°; wall thickness 10mm and outer radius between 40mm and 60mm

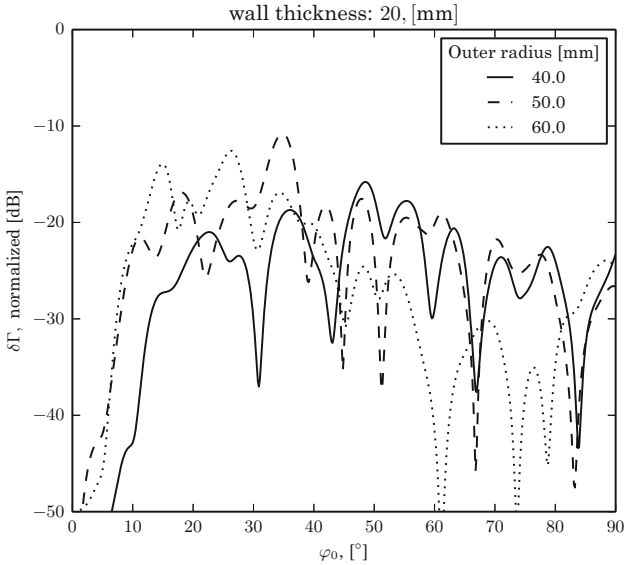

Fig. 6 The signal response $\delta\Gamma$ as a function of the probe position φ_0 for a probe with angle 30°; wall thickness 20 mm and outer radius between 40 and 60 mm

respectively. As noted above the normalization is such that each probe with a particular angle is normalized separately with the maximum value recorded in any figure, so the maximum in each figure is 0 dB. There are differences between the curves in each figure, but the peaks differ only by a few dB and the general trend is that there is a smaller difference between outer radii 50 and 60 mm than between outer radii 40, and 50 mm, particularly in the Fig. 5. It thus is expected that the curves for the largest outer radius 60 mm is not far from that for a plate. For the smallest outer radius 40 mm in Figs. 3, 4, and 5 there is a second peak around $\varphi \approx 65°$ and this is most likely due to a reflection by the inner pipe wall.

Figures 6, 7, and 8 show the same type of curves with the same outer radii but with the doubled wall thickness 20 mm. In these cases the crack is situated further from the scanning surface and the values therefore generally decrease (the normalization is still performed with largest value for a particular probe and these appear in Figs. 3, 4, 5). This decrease is largest in Fig. 8 where the probe angle is 60°. Particularly for the smallest outer radius 40 mm the drop in peak value

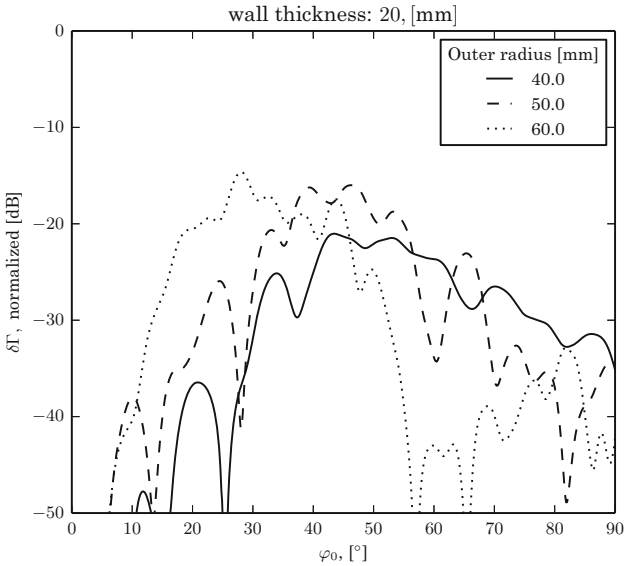

Fig. 7 The signal response $\delta\Gamma$ as a function of the probe position φ_0 for a probe with angle 45°; wall thickness 20 mm and outer radius between 40 and 60 mm

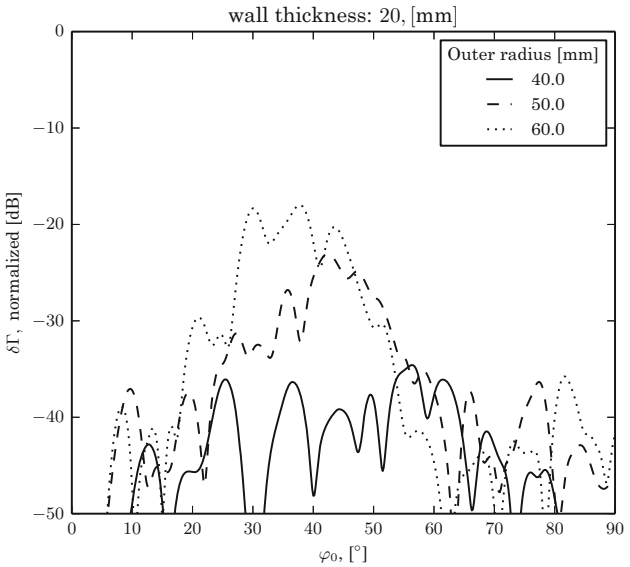

Fig. 8 The signal response $\delta\Gamma$ as a function of the probe position φ_0 for a probe with angle 60°; wall thickness 20 mm and outer radius between 40 and 60 mm

is about 30 dB as compared with the corresponding curve in Fig. 5 for the smaller wall thickness. The reason for this is that the ray from the probe completely misses the crack in this case as it only goes down to the radius 34.6 mm whereas the crack only extends out to 26 mm.

The present results have not been validated with independent results with some other method. One possibility is to perform an experimental investigation and this is of course a very good way. Another way is to perform numerical work by some different method, the method that first comes to mind is the finite element method (FEM), but in the present fully 3D case this will be quite demanding, although it is feasible at least for lower frequencies.

7 Conclusions

This paper gives a model to determine the signal response from an infinite axial crack in a thick-walled pipe. A hypersingular integral equation for the COD is used and it is crucial that the COD is expanded in a system that has the right singularity along the crack edges. A model of an ultrasonic probe on a curved surface is used together with reciprocity to obtain the signal response. As compared to a plate the signals are generally more difficult to interpret, and it is also noted that there is only a finite penetration depth for angled probes in a pipe.

This work shows that there are some interesting effects when investigating the scattering of a crack in an pipe. Thus there is an interest in extending the present work to other crack types in a pipe, as a rectangular (as the present paper but finite in the axial direction), but still axial, crack, or a radial crack.

Acknowledgements This work is supported by the Swedish Radiation Safety Authority (SSM) and this is gratefully acknowledged. The authors would like to thank Associated Professor Per-Å ke Jansson for the help provided.

References

1. Achenbach, J.D.: Wave Propagation in Elastic Solids. North-Holland, New York (1973)
2. Auld, B.A.: General electromechanical reciprocity relations applied to the calculation of elastic wave scattering coefficients. Wave Motion **1**(1), 3–10 (1979). doi:10.1016/0165-2125(79)90020-9
3. Bai, H., Shah, A., Popplewell, N., Datta, S.: Scattering of guided waves by circumferential cracks in steel pipes. Appl. Mech. **68**(4), 619–631 (2001)
4. Benmeddour, F., Treyssède, F., Laguerre, L.: Numerical modeling of guided wave interaction with non-axisymmetric cracks in elastic cylinders. Int. J. Solids Struct. **48**(5), 764–774 (2011)
5. Boström, A., Wirdelius, H.: Ultrasonic probe modeling and nondestructive crack detection. J. Acoust. Soc. Am. **97**(5), 2836–2848 (1995). doi:10.1121/1.411850
6. Boström, A., Kristensson, G., Ström, S.: Transformation properties of plane, spherical and cylindrical scalar and vector wave functions. In: Varadan, V.V., Lakhtakia, A., Varadan, V.K. (eds.) Field Representations and Introduction to Scattering, pp. 165–209. Elsevier, Amsterdam (2000)

7. Bövik, P., Boström, A.: A model of ultrasonic nondestructive testing for internal and subsurface cracks. J. Acoust. Soc. Am. **102**(5), 2723–2733 (1997). doi:10.1121/1.420326
8. Duan, W., Kirby, R.: A numerical model for the scattering of elastic waves from a non-axisymmetric defect in a pipe. Finite Elem. Anal. Des. **100**, 28–40 (2015)
9. Fletcher, S., Lowe, M.J., Ratassepp, M., Brett, C.: Detection of axial cracks in pipes using focused guided waves. J. Nondestruct. Eval. **31**(1), 56–64 (2012)
10. Olsson, S.: Point force excitation of a thick-walled elastic infinite pipe with an embedded inhomogeneity. J. Eng. Math. **28**(4), 311–325 (1994). doi:10.1007/BF00128750
11. Rose, J., Ditri, J., Pilarski, A., Rajana, K., Carr, F.: A guided wave inspection technique for nuclear steam generator tubing. NDT E Int. **27**(6), 307–310 (1994). doi:10.1016/0963-8695(94)90211-9
12. Ström, S.: Introduction to integral representations and integral equations for time-harmonic acoustic, electromagnetic and elastodynamic wave fields. In: Varadan, V.V., Lakhtakia, A., Varadan, V.K. (eds.) Field Representations and Introduction to Scattering, pp. 37–143. Elsevier, Amsterdam (2000)
13. Velichko, A., Wilcox, P.D.: Excitation and scattering of guided waves: relationships between solutions for plates and pipes. J. Acoust. Soc. Am. **125**(6), 3623–3631 (2009)